(μ-Phenoxo)$_2$Co^{II}M^{II} (M = Mn, Co, Zn) Complexes with a Co(salen) Entity in a Macrocyclic Framework: Core Structures and Neighboring M^{II} Effects upon Oxygenation at the Co(salen) Center

Satoru Kita, Hideki Furutachi, and Hisashi Ōkawa*

Department of Chemistry, Faculty of Science, Kyushu University, Hakozaki, Higashiku, Fukuoka 812-8581, Japan

Received August 11, 1998

The phenol-based macrocyclic ligands $(L^{2,3})^{2-}$ and $(L^{2,4})^{2-}$, derived from the [2:1:1] condensation of 2,6-diformyl-4-methylphenol, ethylenediamine, and 1,3-trimethylenediamine or 1,4-tetramethylenediamine, have a salen-like metal-binding site (salen = *N*,*N*′-ethylenedisalicylideneaminate) and a saltn- or salbn-like metal-binding site (saltn = *N*,*N*′-trimethylenedisalicylideneaminate, salbn = *N*,*N*′-tetramethylenedisalicylideneaminate) sharing the phenolic moieties. They form the (μ-phenoxo)$_2$Co^{II}M^{II} complexes [CoMn($L^{2,3}$)(AcO)]ClO_4·DMF (**1**), [CoMn($L^{2,4}$)(AcO)]-ClO_4 (**2**), [CoCo($L^{2,3}$)(AcO)]ClO_4 (**3**), [CoCo($L^{2,4}$)(AcO)]ClO_4 (**4**), [CoZn($L^{2,3}$)(AcO)]ClO_4 (**5**), and [CoZn($L^{2,4}$)-(AcO)]ClO_4 (**6**). Complex **1** crystallizes in the monoclinic space group $P2_1/c$, with $a = 10.027(3)$ Å, $b = 11.713(3)$ Å, $c = 26.821(9)$ Å, $\beta = 93.85(2)°$, $V = 3142(1)$ Å^3, and $Z = 4$. The Co and Mn ions are bridged by the two phenolic oxygens of the macrocycle and an acetate group in the syn-syn mode. The Co^{II} in the salen site is of low-spin and assumes a square-pyramidal geometry with an acetate oxygen at the axial site. The Mn^{II} has a cis six-coordinate geometry with respect to the acetate oxygen and the DMF oxygen. The Mn is displaced 0.955 Å from the basal N_2O_2 least-squares plane. [CoMn($L^{2,4}$)(AcO)]ClO_4·DMF (**2′**) crystallizes in the monoclinic space group $P2_1/c$, with $a = 10.166(5)$ Å, $b = 11.934(4)$ Å, $c = 27.380(8)$ Å, $\beta = 93.97(3)°$, $V = 3313(1)$ Å^3, and $Z = 4$. It has a dinuclear core similar to that of **1**, with square-pyramidal Co^{II} in the salen site and cis six-coordinate Mn^{II} in the salbn site. Complex **3** crystallizes in the triclinic space group $P\bar{1}$, $a = 12.118(3)$ Å, $b = 12.156(2)$ Å, $c = 9.977(1)$ Å, $\alpha = 112.49(1)°$, $\beta = 99.22(2)°$, $\gamma = 77.63(2)°$, $V = 1321.1(5)$ Å^3, and $Z = 2$. Both Co^{II} ions in the salen and saltn sites assume a square-pyramidal geometry with a bridging acetate group in the syn-syn mode. The displacement of the Co in the saltn site, from the basal N_2O_2 least-squares plane toward the apical acetate oxygen, is 0.53 Å. Complex **5** is found to be isostructural with **3**. The complexes **1**, **2**, **4**, **5**, and **6** are reversibly oxygenated in DMF at 0 °C to afford a μ-peroxo dimer complex [{Co^{III}M^{II}(L)(AcO)}$_2$(O_2^{2-})]$^{2+}$. Complex **3** also forms such a μ-peroxo dimer complex but is irreversibly oxidized through an intramolecular-type μ-peroxo complex [Co^{III}Co^{III}($L^{2,3}$)(AcO)(O_2^{2-})]$^+$.

Introduction

The phenol-based macrocyclic compartmental ligands $(L^{m,n})^{2-}$ (Chart 1), possessing two *N*,*N*′-alkylenedisalicylideneaminate entities sharing the phenolic moieties, first obtained by Pilkington and Robson[1] for $m = n = 3$, are now available for a wide range of similar ($m = n$) and dissimilar ($m \neq n$) lateral chains and used for the study of bis(phenoxo)-bridged dinuclear metal complexes.[2,3] The unsymmetric macrocyclic ligands having dissimilar lateral chains are of importance for the study of discrete heterodinuclear, mixed-spin dinuclear, and mixed-valence dinuclear complexes.[4−9] One of our aims in using the unsymmetric macrocycles and their analogues having an additional donor atom on one lateral chain[10,11] or reduced at the imino nitrogens in one N_2O_2 cavity[12−14] is to provide hetero-

Chart 1. Chemical Structures of $(L^{m,n})^{2-}$

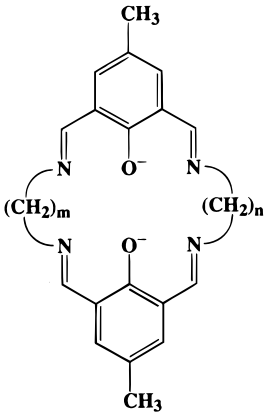

(1) Pilkington, N. H.; Robson, R. *Aust. J. Chem.* **1970**, *23*, 2225.
(2) Tadokoro, N.; Ōkawa, H.; Matsumoto, N.; Koikawa, M.; Kida, S. *J. Chem. Soc., Dalton Trans*. **1991**, 1657. Tadokoro, M.; Sakiyama, H.; Matsumoto, N.; Kodera, M.; Ōkawa, H.; Kida, S. *J. Chem. Soc., Dalton Trans*. **1992**, 313.
(3) Ōkawa, H.; Furutachi, H. *Coord. Chem. Rev*. **1998**, *174*, 51.
(4) Wada, H.; Aono, T.; Motoda, K.; Ohba, M.; Matsumoto, N.; Ōkawa, H. *Inorg. Chim. Acta* **1996**, *246*, 13.
(5) Wada, H.; Motoda, K.; Ohba, M.; Sakiyama, H.; Matsumoto, N.; Ōkawa, H. *Bull. Chem. Soc. Jpn*. **1995**, *68*, 1105.
(6) Aono, T.; Wada, H.; Yonemura, M.; Ohba, M.; Ōkawa, H.; Fenton, D. E. *J. Chem. Soc., Dalton Trans*. **1997**, 1527.
(7) Aono, T.; Wada, H.; Aratake, Y.; Matsumoto, N.; Ōkawa, H.; Matsuda, S. *J. Chem. Soc., Dalton Trans*. **1996**, 25.
(8) Ōkawa, H.; Aratake, Y.; Motoda, K.; Ohba, M.; Sakiyama, H.; Matsumoto, N. *Supramol. Chem*. **1996**, *6*, 293.
(9) Aono, T.; Wada, H.; Yonemura, M.; Furutachi, H.; Ohba, H.; Ōkawa, H. *J. Chem. Soc., Dalton Trans*. **1997**, 3029.

10.1021/ic9809456 CCC: $18.00
Published on Web 08/14/1999

dinuclear cores of functional significance. The metal-binding site formed by the ethylene lateral chain ($m = 2$) is compared to salen (=*N*,*N*′-ethylenedisalicylideneaminate). Because Co(salen) is known for its reactivity toward small molecules such as O_2 and NO,[15,16] the dinuclear Co^{II}M^{II} complexes with Co^{II} in the salen-like metal-binding site of the macrocyles are of great interest regarding the neighboring M^{II} effect upon incorporation and activation of small molecules at the Co(salen) center. In this study, dinuclear Co^{II}M^{II} (M = Mn, Co, Zn) complexes of $(L^{2,3})^{2-}$ and $(L^{2,4})^{2-}$ were synthesized and their crystal structures were determined. The reactivity of the complexes toward molecular dioxygen is studied with respect to the core structure and the neighboring M^{II} ion in the saltn ($n = 3$) or salbn ($n = 4$) site.

Experimental Section

Measurements. Elemental analyses of C, H, and N were obtained at the Elemental Analysis Service Center of Kyushu University. Infrared spectra were recorded on a JASCO IR-810 spectrometer using KBr disks. Molar conductances were measured on a DKK AOL-10 conductivity meter in DMF at 25 °C. Electronic absorption spectra were recorded in DMF on a Shimadzu MPS-2000 spectrometer. Magnetic susceptibilities were measured on a Faraday balance in the temperature range 80−300 K. Calibrations were made using $[Ni(en)_3]S_2O_3$,[17] and diamagnetic corrections were made using Pascal's constants.[18] X-band ESR spectra were recorded on a JEOL JEX-FE3X spectrometer. Fast-atom bombardment (FAB) mass spectra were obtained on a JMSSX/SX 102A tandem mass spectrometer using *m*-nitrobenzyl alcohol as the matrix. ^{1}H and ^{13}C NMR spectra were recorded on a JEOL JNM-GX 400 spectrometer using tetramethylsilane as the internal standard. Cyclic voltammograms were measured using a BAS CV-50W electrochemical analyzer in DMF solution containing tetra-*n*-butylammonium perchlorate (TBAP) as the supporting electrolyte (**Caution!** TBAP is explosive and should be handled with great care). A three-electrode cell was used which was equipped with a glassy carbon working electrode, a platinum coil as the counter electrode, and a Ag/Ag$^+$(TBAP/acetonitrile) reference electrode.

Materials. Unless otherwise stated, all reagents were purchased from commercial sources and used without further purification. 2,6-Diformyl-4-methylphenol was prepared by a literature method.[19] Solvents were dried and purified by standard methods.

Preparations. All operations for syntheses were carried out in a nitrogen atmosphere using a model MO-40-IV glovebox from Vacuum Atmospheres Co. or in an argon atmosphere using a standard Schlenk apparatus.

[Pb{Co(L^{2,3})}$_2$](ClO$_4$)$_2$·2CH$_3$OH. A methanol solution (5 cm^3) of lead(II) perchlorate trihydrate (1.11 g, 2.42 mmol) was added to a suspension of (*N*,*N*′-ethylenebis(3-formyl-5-methylsalicylideneaminato))cobalt(II) (1.99 g, 4.84 mmol) in methanol (30 cm^3), and the mixture was stirred at room temperature for 30 min. To the resulting red solution was added dropwise a methanol solution (10 cm^3) of 1,3-trimethylenediamine (0.36 g, 2.42 mmol), and the mixture was stirred at ambient temperature for 2 h to form brown microcrystals. Yield: 2.33 g (74%). Anal. Calcd for $C_{48}Cl_2Co_2H_{56}N_8O_{14}Pb$: C, 42.12; H, 3.90; N, 8.48. Found: C, 42.24; H, 4.14; N, 8.21. Selected IR (KBr) [ν/cm^{-1}]: 2910, 2850, 1630, 1100, 1090, 620.

[Pb{Co(L^{2,4})}$_2$](ClO$_4$)$_2$·2CH$_3$OH. This was obtained as brown microcrystals similarly to [Pb{Co(L^{2,3})}$_2$](ClO$_4$)$_2$·2CH$_3$OH using 1,4-tetramethylenediamine instead of 1,3-trimethylenediamine. Yield: 64%. Anal. Calcd. for $C_{50}Cl_2Co_2H_{60}N_8O_{14}Pb$: C, 43.13; H, 4.12; N, 8.01. Found: C, 43.11; H, 4.34; N, 8.04. Selected IR (KBr) [ν/cm^{-1}]: 2910, 2850, 1620, 1100, 1090, 620.

[CoMn(L^{2,3})(AcO)]ClO$_4$·DMF (1). A methanol solution (15 cm^3) of manganese(II) perchlorate hexahydrate (54.3 mg, 0.15 mmol), manganese(II) sulfate hexahydrate (39.0 mg, 0.15 mmol), and sodium acetate (24.6 mg, 0.30 mmol) was added to a suspension of [Pb{Co(L^{2,3})}$_2$](ClO$_4$)$_2$·2CH$_3$OH (205 mg, 0.15 mmol) in methanol (10 cm^3), and the mixture was stirred at ambient temperature for 1 h. The precipitate of $PbSO_4$ was removed by filtration, and the filtrate was evaporated to dryness. The residue was dissolved in DMF, and the solution was diffused with 2-propanol to give red crystals. Yield: 106 mg (48%). Anal. Calcd for $C_{28}ClCoH_{34}MnN_5O_9$: C, 45.82; H, 4.67; N, 9.54. Found: C, 45.16; H, 4.99; N, 9.61. FAB mass: *m*/*z* 561.1 for {CoMn(L^{2,3})(AcO)}$^+$. μ_{eff} per CoMn: 6.31 μ_B at 298 K. Selected IR (KBr) [ν/cm^{-1}]: 2930, 2850, 1630, 1560, 1400, 1110, 1080, 620. Molar conductance [Λ_M/S cm^2 mol^{-1}] in DMF: 57.5. UV−vis data [λ_{max}/nm (ϵ/M^{-1} cm^{-1})] in DMF: 355 (12 100), 440 (sh), 560 (1820).

[CoMn(L^{2,4})(AcO)]ClO$_4$ (2). This complex was synthesized as red crystals in similarly to **1**, using [Pb{Co(L^{2,4})}$_2$](ClO$_4$)$_2$·2CH$_3$OH instead of [Pb{Co(L^{2,3})}$_2$](ClO$_4$)$_2$·2CH$_3$OH. Yield: 59%. Anal. Calcd for $C_{26}ClH_{29}CoMnN_4O_8$: C, 46.27; H, 4.33; N, 8.30. Found: C, 46.35; H, 4.41; N, 8.32. FAB mass: *m*/*z* 575.1 for {CoMn(L^{2,4})(AcO)}$^+$. μ_{eff} per CoMn: 5.98 μ_B at 298 K. Selected IR (KBr) [ν/cm^{-1}]: 2935, 2860, 1630, 1560, 1400, 1100, 1060, 620. Molar conductance [Λ_M/S cm^2 mol^{-1}] in DMF: 60.1. UV−vis data [λ_{max}/nm (ϵ/M^{-1} cm^{-1})] in DMF: 365 (13 750), 460 (sh), 555 (1750).

A portion of **2** dissolved in methanol was treated with an excess of KPF_6. The resulting precipitate of $KClO_4$ was removed by filtration, and the filtrate was evaporated to dryness. The residue was crystallized from DMF/2-propanol as [CoMn(L^{2,4})(AcO)]PF$_6$·DMF (**2′**) suitable for X-ray crystallography. Anal. Calcd. for $C_{29}CoF_6H_{36}MnN_5O_5P$: C, 43.90; H, 4.57; N, 8.83. Found: C, 44.28; H, 4.53; N, 8.82.

[CoCo(L^{2,3})(AcO)]ClO$_4$ (3). This was obtained as red crystals by the reaction of [Pb{Co(L^{2,3})}$_2$](ClO$_4$)$_2$·2CH$_3$OH (205 mg, 0.15 mmol) with cobalt(II) perchlorate hexahydrate (54.9 mg, 0.15 mmol), cobalt(II) sulfate heptahydrate (42.3 mg, 0.15 mmol), and sodium acetate (24.6 mg, 0.30 mmol) in methanol (30 cm^3). Yield: 100 mg (50%). Anal. Calcd for $C_{25}ClCo_2H_{27}N_4O_8$: C, 45.05; H, 4.21; N, 8.47. Found: C, 45.16; H, 4.09; N, 8.43. FAB mass: *m*/*z* 565.1 for {CoCo(L^{2,3})(AcO)}$^+$. μ_{eff} per CoCo: 5.04 μ_B at 298 K. Selected IR (KBr) [ν/cm^{-1}]: 2930, 2850, 1630, 1560, 1450, 1110, 1080, 620. Molar conductance [Λ_M/S cm^2 mol^{-1}] in DMF: 69. UV−vis data [λ_{max}/nm (ϵ/M^{-1} cm^{-1})] in DMF: 360 (11 320), 465 (sh), 550 (1410).

[CoCo(L^{2,4})(AcO)]ClO$_4$ (4). This was synthesized as red crystals similarly to **3**, using [Pb{Co(L^{2,4})}$_2$](ClO$_4$)$_2$·2CH$_3$OH instead of [Pb{Co(L^{2,3})}$_2$](ClO$_4$)$_2$·2CH$_3$OH. Yield: 55%. Anal. Calcd for $C_{26}ClCo_2H_{29}N_4O_8$: C, 46.00; H, 4.38; N, 8.24. Found: C, 46.00; H, 4.31; N, 8.25. FAB mass: *m*/*z* 579.1 for {CoCo(L^{2,4})(AcO)}$^+$. μ_{eff} per

(10) (a) Ōkawa, H.; Nishio, J.; Ohba, M.; Tadokoro, M.; Matsumoto, N.; Koikawa, M.; Kida, S.; Fenton, D. E. *Inorg. Chem.* **1993**, *32*, 2949. (b) Nishio, J.; Ōkawa, H.; Ohtsuka, S.; Tomono, M. *Inorg. Chim. Acta* **1994**, *218*, 27. (c) Shimoda, J.; Furutachi, H.; Yonemura, M.; Ohba, M.; Matsumoto, N.; Ōkawa, H. *Chem. Lett.* **1996**, 979. (d) Furutachi, H.; Ōkawa, H. *Inorg. Chem.* **1997**, *36*, 3911. (e) Furutachi, H.; Ōkawa, H. *Bull. Chem. Soc. Jpn.* **1998**, *71*, 671. (f) Yamami, M.; Furutachi, H.; Ōkawa, H. *Chem. Lett.* **1988**, 211.

(11) Ohtsuka, S.; Kodera, M.; Motoda, K.; Ohba, M.; Ōkawa, H. *J. Chem. Soc., Dalton Trans.* **1995**, 2599.

(12) (a) Yonemura, M.; Matsumura, Y.; Ohba, M.; Ōkawa, H.; Fenton, D. E. *Chem. Lett.*, **1996**, 601. (b) Yonemura, M.; Matsumura, Y.; Furutachi, H.; Ohba, M.; Ōkawa, H.; Fenton, D. E. *Inorg. Chem.* **1997**, *36*, 2711. (c) Yonemura, M.; Ohba, M.; Takahashi, K.; Ōkawa, H.; Fenton, D. E. *Inorg. Chim. Acta*, in press.

(13) Fraser, C.; Johnston, S. L.; Rheingold, A. L.; Haggerty, B. S.; Williams, G. K.; Whelan, J.; Bosnich, B. *Inorg. Chem.* **1992**, *31*, 1835. McCollum, D. G.; Yap, G. P. A.; Rheingold, A. L.; Bosnich, B. *J. Am. Chem. Soc.* **1996**, *118*, 1365 and references therein.

(14) Karunakaran, S.; Kandaswamy, M. *J. Chem. Soc., Dalton Trans.* **1994**, 1595.

(15) (a) Ochiai, E. *J. Inorg. Nucl. Chem.* **1973**, *35*, 1727. (b) Jones, R. D.; Summerville, D. A.; Basolo, F. *Chem. Rev.* **1979**, *79*, 139. (c) McLendon, G.; Martell, A. E. *Coord. Chem. Rev.* **1976**, *19*, 1.

(16) (a) Tamaki, M.; Masuda, I.; Shinra, R. *Bull. Chem. Soc. Jpn.* **1969**, *42*, 2858. (b) Earnshaw, A.; Hewlett, P. C.; Larkworthy, L. F. *J. Chem. Soc.* **1965**, 4718. (c) Bultitude, J.; Larkworthy, L. F.; Mason, J.; Povey, D. C.; Sandell, B. *Inorg. Chem.* **1984**, *23*, 3629. (d) Duffin, P. A.; Larkworthy, L. F.; Mason, J.; Stephens, A. N.; Thompson, R. M. *Inorg. Chem.* **1987**, *26*, 2034.

(17) Curtis, N. F. *J. Chem. Soc.* **1961**, 3147.

(18) Boudreaux, E. A.; Mulay, L. N. *Theory and Applications of Molecular Paramagnetism*; Wiley: New York 1976; pp 491−494.

(19) Denton, D. A.; Suschitzky, H. *J. Chem. Soc.* **1963**, 4741.

Table 1. Crystal Data for **1**, **2**, **3** and **5**

	1	**2′**	**3**	**5**
formula	$C_{28}H_{34}N_5O_9ClCoMn$	$C_{29}H_{36}N_5O_5PF_6CoMn$	$C_{25}H_{27}N_4O_8ClCo_2$	$C_{25}H_{27}N_4O_8ClCoZn$
fw	733.93	793.47	664.83	671.28
crystal color	red	red	red	red
crystal size	0.20 × 0.20 × 0.20	0.20 × 0.20 × 0.20	0.40 × 0.50 × 0.30	0.25 × 0.30 × 0.25
crystal system	monoclinic	monoclinic	triclinic	triclinic
space group	$P2_1/c$ (No. 14)	$P2_1/c$ (No. 14)	$P\bar{1}$ (No. 2)	$P\bar{1}$ (No. 2)
a/Å	10.027 (3)	10.166 (5)	12.118 (3)	12.097(3)
b/Å	11.713 (3)	11.934 (3)	12.156 (2)	12.209(5)
c/Å	26.821 (9)	27.380 (6)	9.977 (1)	9.977(4)
α/deg	90	90	112.49 (1)	112.29(3)
β/deg	93.85(2)	93.97(3)	99.22 (2)	99.19(3)
γ/deg	90	90	77.63 (2)	77.69(3)
V/Å^3	3142(1)	3313(1)	1321.3 (5)	1327.0(9)
Z	4	4	2	2
μ(MoKα)/cm^{-1}	10.74	10.10	14.14	16.87
D_c/g cm^{-3}	1.551	1.590	1.671	1.680
no. of reflns	7981	8445	4764	4926
F(000)	1512.00	1624.00	680.000	686.000
R^a	0.054	0.048	0.038	0.045
$R_w{}^{b,c}$	0.090	0.034	0.025	0.031

[a] $R = \sum||F_o| - |F_c||/\sum|F_o|$. [b] $R_w = \{\sum[w(|F_o| - |F_c|)^2]/\sum[w|F_o|^2]\}^{1/2}$. [c] $w = 1/\sigma^2(F_o)$.

CoCo: 4.91 μ_B at 298 K. Selected IR (KBr) [ν/cm^{-1}]: 2935, 2860, 1640, 1560, 1460, 1110, 1060, 625. Molar conductance [Λ_M/S cm^2 mol^{-1}] in DMF: 67. UV−vis data [λ_{max}/nm (ϵ/M^{-1} cm^{-1})] in DMF: 370 (10 960), 460 (sh), 540 (1550).

[CoZn(L^{2,3})(AcO)]ClO$_4$ (5). This was prepared as red crystals similarly to **1**, using zinc(II) perchlorate hexahydrate, zinc(II) sulfate heptahydrate, and sodium acetate. Yield: 50%. Anal. Calcd for $C_{25}ClCoH_{27}N_4O_8Zn$: C, 44.75; H, 4.08; N, 8.37. Found: C, 44.73; H, 4.05; N, 8.35. FAB mass: m/z 570.1 for {CoZn(L^{2,3})(AcO)}$^+$. μ_{eff} per CoZn: 2.30 μ_B at 298 K. Selected IR (KBr) [ν/cm^{-1}]: 2910, 2850, 1620, 1560, 1450, 1120, 1110, 1080, 620. Molar conductance [Λ_M/S cm^2 mol^{-1}] in DMF: 60. UV−vis data [λ_{max}/nm (ϵ/M^{-1} cm^{-1})] in DMF: 360 (11 220), 440 (sh), 550 (2160).

[CoZn(L^{2,4})(AcO)]ClO$_4$ (6). This complex was synthesized as red crystals. Yield: 56%. Anal. Calcd for $C_{26}ClCoH_{29}N_4O_8Zn$: C, 45.64; H, 4.32; N, 8.24. Found: C, 45.57; H, 4.27; N, 8.18. FAB mass: m/z 584.2 for {CoZn(L^{2,4})(AcO)}$^+$. μ_{eff} per CoZn: 1.90 μ_B at 298 K. Selected IR (KBr) [ν/cm^{-1}]: 2930, 2860, 1630, 1560, 1460, 1100, 1060, 620. Molar conductance [Λ_M/S cm^2 mol^{-1}] in DMF: 71. UV−vis data [λ_{max}/nm (ϵ/M^{-1} cm^{-1})] in DMF: 365 (13 750), 460 (sh), 550 (2140).

X-ray Crystallography. Each single crystal of [CoMn(L^{2,3})(AcO)]ClO$_4$·DMF (**1**), [CoMn(L^{2,4})(AcO)]PF$_6$·DMF (**2′**), [CoCo(L^{2,3})(AcO)]ClO$_4$ (**3**), and [CoZn(L^{2,3})(AcO)]ClO$_4$ (**5**) was mounted on a glass fiber, coated with epoxy resin, and used for data collection on a Rigaku AFC7R diffractometer, using graphite-monochromated Mo Kα radiation (λ = 0.710 69 Å) and a 12 kW rotating anode generator at 293 K. For intensity data collections, the $\omega-2\theta$ scan technique was used to a maximum 2θ value of 50.0° at scan speed 16.0°/min (in ω). The weak reflections ($I < 10.0\sigma(I)$) were rescanned (maximum of four scans), and the counts were accumulated to ensure good counting statistics. Stationary-background counts were recorded on each side of the reflection. The ratio of peak counting time to background counting time was 2:1. The diameter of the incident-beam collimator was 1.0 mm, the crystal-to-detector distance was 235 mm, and the computer-controlled detector aperture was set to 9.0 × 13.0 mm (horizontal × vertical). The cell parameters were detemined by 25 reflections in the 2θ ranges 29.74° ≤ 2θ ≤ 30.74° for **1**, 29.10° ≤ 2θ ≤ 29.96° for **2′**, 20.11° ≤ 2θ ≤ 24.31° for **3**, and 29.80° ≤ 2θ ≤ 29.97° for **5**. The intensities of the representative reflections were measured after every 150 reflections. Over the course of the data collection, the standards decreased by −0.5% for **1**, by −1.0% for **2′**, by −1.9% for **3**, and by −0.3% for **5**. A linear correction factor was applied to the data to account for the phenomenon. The linear absorption coefficient, μ, for Mo Kα radiation was 10.7 cm^{-1} for **1**, 10.1 cm^{-1} for **2′**, 14.1 cm^{-1} for **3**, and 16.9 cm^{-1} for **5**. An empirical absorption correction based on azimuthal scans of several reflections was applied which resulted in transmission factors ranging from 0.80 to 1.00 for **1**, from 0.92 to 1.00 for **2′**, from 0.75 to 1.00 for **3**, and from 0.83 to 1.00 for **5**. Intensity data were corrected for Lorentz and polarization effects. Crystal data for **1**, **2**, **3**, and **5** are given in Table 1.

The structures were solved by direct methods and expanded using Fourier techniques. Non-hydrogen atoms were refined anisotropically. Hydrogen atoms were included in structure factor calculations. The final cycle of full-matrix least-squares refinement of **1**, **2′**, **3**, and **5** was based on 5370, 4554, 3606, and 3995 observed reflections ($I > 3.00\sigma(I)$), respectively, and 434, 452, 362, and 362 variable parameters, respectively. Unweighted and weighted agreement factors of the forms $R = \sum||F_o| - |F_c||/\sum|F_o|$ and $R_w = [(\sum w(|F_o| - |F_c|)^2/\sum w|F_c|^2]^{1/2}$ are used. The agreement factors R (R_w) of **1**, **2′**, **3**, and **5** were 0.054 (0.090), 0.048 (0.034), 0.038 (0.025), and 0.045 (0.031), respectively.

The neutral-atom scattering factors were taken from Cromer and Waber.[20] Anomalous dispersion effects were included in F_c; the values for $\Delta f'$ and $\Delta f''$ were those of Creagh and McAuley.[21] The values for the mass attenuation coefficients were those of Creagh and Hubbel.[22] All calculations were performed using the TEXSAN[23] crystallographic software from Molecular Structure Corp.

Results and Discussion

Preparation. In our previous studies,[2] the macrocyclic ligands were synthesized by a stepwise template reaction as trinuclear Cu^{II}Pb^{II}Cu^{II} and Ni^{II}Pb^{II}Ni^{II} complexes, [Pb{Cu(L^{m,n})}$_2$]X$_2$ and [Pb{Ni(L^{m,n})}$_2$]X$_2$, where the Cu^{II} or Ni^{II} ion in the {M(L^{m,n})} moiety occupies one of the N_2O_2 cavities (smaller cavity) and the remaining N_2O_2 cavity is provided for sandwiching the Pb^{II} ion. The trinuclear complexes could be converted into dinuclear complexes, [Cu^{II}M^{II}(L^{m,n})]X$_2$ and [Ni^{II}M^{II}(L^{m,n})]X$_2$, by the reaction with MSO$_4$·nH$_2$O and MX$_2$·nH$_2$O in an appropriate solvent.[4−9] In this reaction, Pb^{II} was deposited as insoluble PbSO$_4$, and the desired dinuclear complexes were obtained in good yields from the Pb-separated solution. This method was successfully applied to the synthesis of Co^{II}M^{II} complexes in this study. The trinuclear Co^{II}Pb^{II}Co^{II} complexes, [Pb{Co-

(20) Cromer, D. T.; Waber, J. T. *International Tables for X-ray Crystallography*; Kynoch Press: Birmingham, U.K., 1974; Vol. IV.
(21) Creagh, D. C.; McAuley, W. J. In *International Tables for X-ray Crystallography*; Wilson, A. J. C., et al., Eds.; Kluwer: Boston, MA, 1992; pp 219−222.
(22) Creagh, D. C.; Hubbell, H. H. In *International Tables for X-ray Crystallography*; Wilson, A. J. C., et al., Eds.; Kluwer: Boston, MA, 1992; pp 200−206.
(23) *TEXSAN*; Molecular Structure Corp.: Houston, TX, 1985.

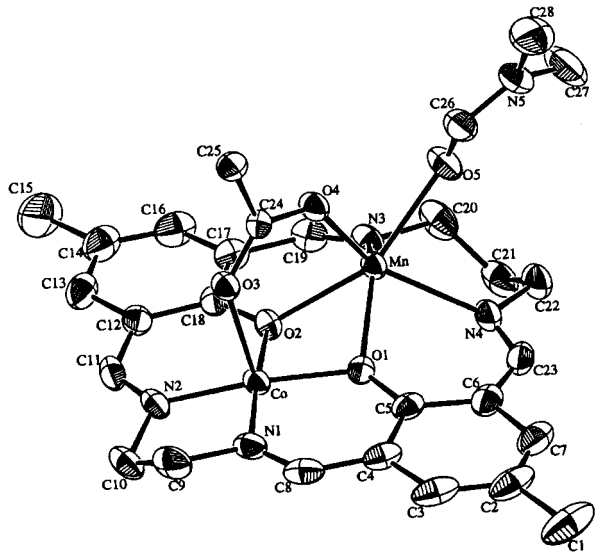

Figure 1. ORTEP view of **1** with the numbering scheme.

Table 2. Relevant Bond Distances (Å) and Angles (deg) for **1**

	Distances		
Co−O(1)	1.886(3)	Co−O(2)	1.899(3)
Co−O(3)	2.148(3)	Co−N(1)	1.863(4)
Co−N(2)	1.873(3)	Mn−O(1)	2.188(3)
Mn−O(2)	2.230(3)	Mn−O(4)	2.102(3)
Mn−O(5)	2.220(3)	Mn−N(3)	2.200(4)
Mn−N(4)	2.237(4)	Co−Mn	3.108(1)
	Angles		
O(1)−Co−O(2)	83.3(1)	O(1)−Co−O(3)	98.3(1)
O(1)−Co−N(1)	94.7(1)	O(1)−Co−N(2)	171.2(1)
O(2)−Co−O(3)	92.9(1)	O(2)−Co−N(1)	173.3(1)
O(2)−Co−N(2)	94.5(1)	O(3)−Co−N(1)	93.7(1)
O(3)−Co−N(2)	90.3(1)	N(1)−Co−N(2)	86.6(2)
O(1)−Mn−O(2)	69.4(1)	O(1)−Mn−O(4)	91.3(1)
O(1)−Mn−O(5)	136.7(1)	O(1)−Mn−N(3)	131.3(1)
O(1)−Mn−N(4)	78.6(1)	O(2)−Mn−O(4)	89.3(1)
O(2)−Mn−O(5)	151.6(1)	O(2)−Mn−N(3)	78.1(1)
O(2)−Mn−N(4)	123.5(1)	O(4)−Mn−O(5)	80.3(1)
O(4)−Mn−N(3)	124.1(1)	O(4)−Mn−N(4)	137.7(1)
O(5)−Mn−N(3)	86.0(1)	O(5)−Mn−N(4)	79.7(1)
N(3)−Mn−N(4)	91.1(2)	Co−O(1)−Mn	99.2(1)
Co−O(2)−Mn	97.3(1)		

$(L^{2,3})\}_2](ClO_4)_2\cdot 2CH_3OH$ and $[Pb\{Co(L^{2,4})\}_2](ClO_4)_2\cdot 2CH_3OH$, were prepared by the reaction of (*N*,*N*′-ethylenebis(3-formyl-5-methylsalicylideneaminato))cobalt(II) with 1,3-trimethylenediamine and 1,4-tetramethylenediamine, respectively, in the presence of lead(II) perchlorate trihydrate. The resulting Co^{II}-Pb^{II}Co^{II} complexes were then converted into the Co^{II}M^{II} perchlorate complexes (M = Mn, Co, Zn; **1**−**6**) by reaction with $MSO_4\cdot nH_2O$ and $M(ClO_4)_2\cdot nH_2O$ in methanol. All the synthetic operations were carried out in an atmosphere of nitrogen because the precursor Co^{II}Pb^{II}Co^{II} complexes and the Co^{II}M^{II} complexes (**1**−**6**) are all air-sensitive.

Crystal Structures. (a) [CoMn(L^{2,3})(AcO)]ClO$_4$·DMF (1). An ORTEP[24] view of **1** is given in Figure 1 together with the numbering scheme. Relevant bond distances and angles are given in Table 2.

The Co^{II} and Mn^{II} ions are bridged by the phenolic oxygens O(1) and O(2) of the macrocycle and the acetate oxygens O(3) and O(4) in the syn-syn mode. The Co- -Mn intermetallic separation is 3.108(1) Å. The Co in the salen site assumes a square-pyramidal geometry with N(1), N(2), O(1), and O(2) of the macrocycle on the base and O(3) of the acetate bridge at the apical site. The basal Co-to-macrocycle bond distances fall in the range 1.863(4)−1.899(3) Å values that are common for low-spin Co(II).[25] The apical Co−O(3) bond is significantly elongated (2.148(3) Å). The Co deviates by 0.125 Å from the basal least-squares plane toward O(3).

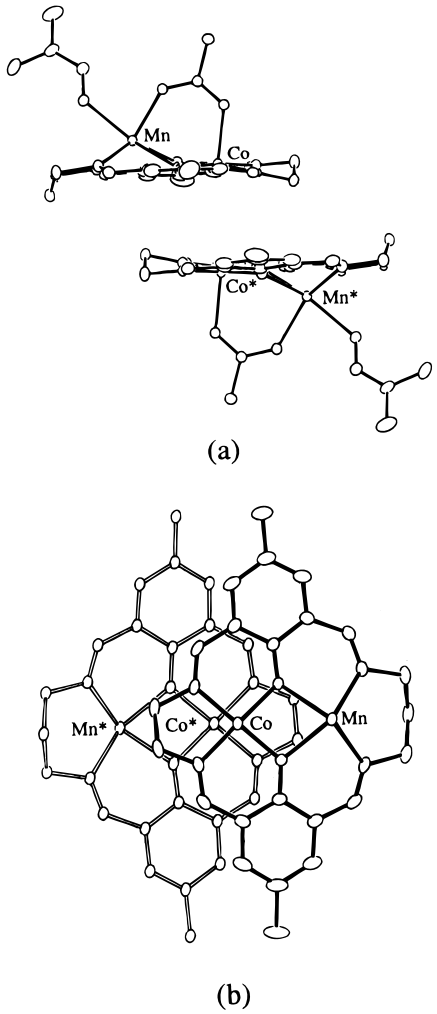

Figure 2. Edge view (a) and top view (b) of the stacking mode of **1**.

The Mn in the saltn site has a six-coordinate geometry together with O(4) of the bridging acetate group and O(5) of the DMF ligand. The exogenous donor atoms O(4) and O(5) are situated cis with respect to the mean plane defined by O(1), O(2), N(3), and N(4). The cis six-coordinate geometry arises from the mismatch between the large ionic radius of Mn^{II} and the cavity size of the saltn site. The Mn-to-macrocycle bond distances range from 2.188(3) to 2.237(4) Å, which are common for high-spin Mn^{II} ion. The Mn−O(4) (acetate) bond distance is rather short (2.102(3) Å). The Mn deviates 0.955 Å from the least-squares plane defined by O(1), O(2), N(3), and N(4).

In the bulk, the two $[CoMn(L^{2,3})(AcO)]^+$ cations stack with each other at the open face of the Co(salen) entity. An edge view and a top view of the stacking mode are shown in Figure 2. The Co- -Co′ separation in the stack is 3.808(1) Å, which is shorter than the intermolecular Co- -O(1′) separation (4.331(3) Å). The stacking mode differs from the out-of-plane bonding through the phenolic oxygen as found for dimeric [Co(salen)]$_2$.[26,27]

(24) Johnson, C. K. Report 3794; Oak Ridge National Laboratory: Oak Ridge, TN, 1965.

(25) Calligaris, M.; Nardin, G.; Randaccio, L. *Coord. Chem. Rev.* **1972**, *7*, 385.

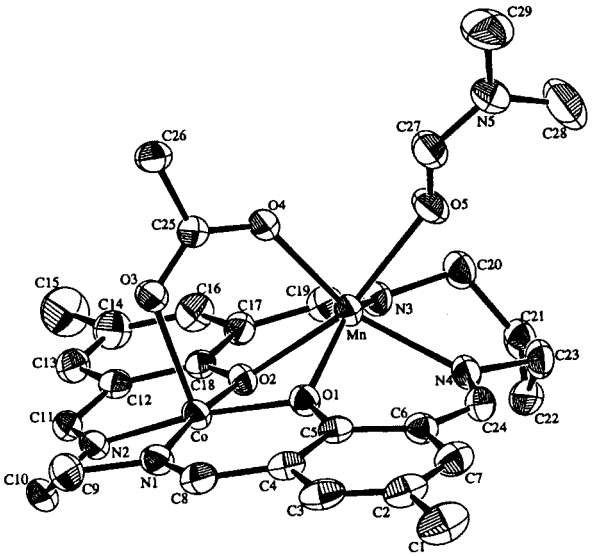

Figure 3. ORTEP view of **2** with the numbering scheme.

Table 3. Relevant Bond Distances (Å) and Angles (deg) for **2**

	Distances		
Co−O(1)	1.899(3)	Co−O(2)	1.915(3)
Co−O(3)	2.143(3)	Co−N(1)	1.865(4)
Co−N(2)	1.866(4)	Mn−O(1)	2.186(3)
Mn−O(2)	2.244(3)	Mn−O(4)	2.109(3)
Mn−O(5)	2.188(3)	Mn−N(3)	2.232(4)
Mn−N(4)	2.261(4)	Co−Mn	3.120(1)
	Angles		
O(1)−Co−O(2)	83.7(1)	O(1)−Co−O(3)	97.8(1)
O(1)−Co−N(1)	94.5(2)	O(1)−Co−N(2)	170.8(1)
O(2)−Co−O(3)	92.9(1)	O(2)−Co−N(1)	173.6(1)
O(2)−Co−N(2)	95.0(1)	O(3)−Co−N(1)	93.4(1)
O(3)−Co−N(2)	91.4(1)	N(1)−Co−N(2)	85.8(2)
O(1)−Mn−O(2)	70.1(1)	O(1)−Mn−O(4)	90.8(1)
O(1)−Mn−O(5)	130.0(1)	O(1)−Mn−N(3)	139.9(1)
O(1)−Mn−N(4)	77.6(1)	O(2)−Mn−O(4)	87.8(1)
O(2)−Mn−O(5)	156.1(1)	O(2)−Mn−N(3)	79.8(1)
O(2)−Mn−N(4)	122.1(1)	O(4)−Mn−O(5)	80.1(1)
O(4)−Mn−N(3)	114.5(1)	O(4)−Mn−N(4)	140.0(1)
O(5)−Mn−N(3)	86.5(1)	O(5)−Mn−N(4)	78.9(1)
N(3)−Mn−N(4)	97.7(1)	Co−O(1)−Mn	99.3(1)
Co−O(2)−Mn	96.9(1)		

(b) [CoMn(L^{2,4})(AcO)]PF$_6$·DMF (2′). An ORTEP view of **2′** is given in Figure 3 together with the numbering scheme. Relevant bond distances and angles are given in Table 3.

The dinuclear core of **2′** is essentially similar to that of **1**, with the Co^{II} in the salen site and the Mn^{II} in the salbn site. The Co- -Mn intermetallic separation, bridged by the phenolic oxygens O(1) and O(2) and the acetate oxygens O(3) and O(4) in the syn-syn mode, is 3.120(1) Å. The geometry about the Co^{II} is square-pyramidal with the acetate oxygen O(3) at the axial site. The in-plane Co−N and Co−O bond distances are in the range 1.865(4)−1.915(3) Å. The axial Co−O(3) bond distance is slightly longer (2.143(3) Å). The Co^{II} is displaced 0.128 Å from the basal N_2O_2 least-squares plane toward O(3).

The Mn^{II} in the salbn site has a cis six-coordinate geometry with respect to the exogenous donor oxygens O(4) and O(5). The Mn deviates 0.874 Å from the basal least-squares plane defined by O(1), O(2), N(3), and N(4). The deviation is smaller than that for **1** (0.955 Å) because of the large cavity size of the salbn site relative to the saltn site.

(26) Bruckner, S.; Calligaris, M.; Nardun, G.; Randaccio, L. *Acta Crystallogr., Sect. B* **1969**, *25*, 1671.
(27) de Iasi, R.; Post, B.; Holt, S. L. *Inorg. Chem.* **1971**, *10*, 1498.

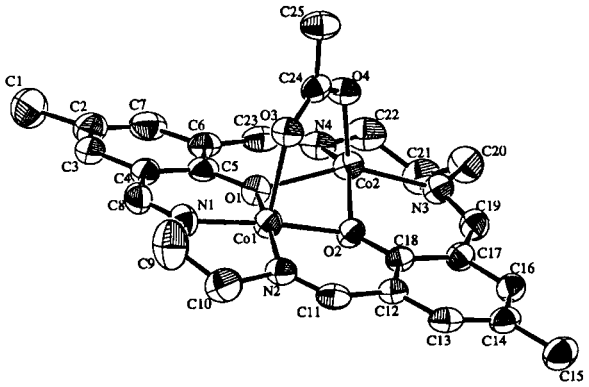

Figure 4. ORTEP view of **3** with the numbering scheme.

Table 4. Relevant Bond Distances (Å) and Angles (deg) for **3** and **5**[a]

	3 (M = Co)	**5** (M = Zn)
	Distances	
Co−O(1)	1.895(2)	1.901(2)
Co−O(2)	1.898(2)	1.893(2)
Co−O(3)	2.138(2)	2.142(3)
Co−N(1)	1.860(3)	1.845(3)
Co−N(2)	1.867(3)	1.878(3)
M−O(1)	2.064(2)	2.084(3)
M−O(2)	2.045(2)	2.089(3)
M−O(4)	1.981(2)	1.969(3)
M−N(3)	2.025(3)	2.025(3)
M−N(4)	2.059(3)	2.072(3)
Co−M	2.972(8)	2.987(1)
	Angles	
O(1)−Co−O(2)	81.60(10)	81.6(1)
O(1)−Co−O(3)	91.18(9)	91.2(1)
O(1)−Co−N(1)	94.1(1)	94.7(1)
O(1)−Co−N(2)	168.8(1)	167.7(1)
O(2)−Co−O(3)	92.95(9)	93.0(1)
O(2)−Co−N(1)	172.5(1)	171.6(1)
O(2)−Co−N(2)	94.5(1)	94.1(1)
O(3)−Co−N(1)	93.8(1)	94.5(1)
O(3)−Co−N(2)	99.6(1)	100.6(1)
N(1)−Co−N(2)	87.8(1)	88.0(2)
O(1)−M−O(2)	74.18(9)	72.87(9)
O(1)−M−O(4)	92.69(9)	95.6(1)
O(1)−M−N(3)	150.9(1)	146.8(1)
O(1)−M−N(4)	85.5(1)	85.2(1)
O(2)−M−O(4)	98.17(9)	99.79(10)
O(2)−M−N(3)	87.7(1)	86.3(1)
O(2)−M−N(4)	144.8(1)	142.7(1)
O(4)−M−N(3)	112.7(1)	113.6(1)
O(4)−M−N(4)	111.5(1)	112.3(1)
N(3)−M−N(4)	97.5(1)	97.2(1)
Co−O(1)−M	97.2(1)	97.0(1)
Co−O(2)−M	97.8(1)	97.1(1)

[a] Co and M in the table mean the salen and saltn sites, respectively.

In the bulk, the two [CoMn(L^{2,4})(AcO)]$^+$ cations stack with each other at the open face of the Co(salen) entity. The Co- -Co′ separation in the stack is 3.855(2) Å.

(c) [CoCo(L^{2,3})(AcO)]ClO$_4$ (3) and [CoZn(L^{2,3})(AcO)]ClO$_4$ (5). These complexes are isostructural. The crystal structure for **3** is discussed in detail. An ORTEP[21] view of **3** is shown in Figure 4 together with the numbering scheme. The selected bond distances and angles of **3** and **5** are given in Table 4.

The two Co ions in **3** are bridged by the phenolic oxygens O(1) and O(2) of the macrocycle and the acetate oxygens O(3) and O(4) in the syn-syn mode. The Co(1)- -Co(2) intermetallic separation is 2.972(8) Å. The Co(1) in the salen site assumes a square-pyramidal geometry together with O(3) of the acetate bridge at the apical site. The basal Co-to-macrocycle bond

distances fall in the range 1.860(3)−1.898(2) Å. The apical Co(1)−O(3) bond is elongated (2.138(2) Å). The Co(1) is 0.15 Å deviated from the basal least-squares plane toward O(3).

The Co(2) in the saltn site has a five-coordinate geometry along with O(4) of the bridging acetate group. The geometry about the metal can be described as a distorted square-pyramid with the N_2O_2 donor atoms of the macrocycle on the base and the acetate oxygen at the apex. The discriminating factor τ[28] ($\tau = 0$ for a square-pyramid and $\tau = 1$ for a trigonal-bipyramid) is 0.102 for this metal. The Co(2) deviates 0.53 Å from the basal least-squares plane toward O(4). The basal Co-to-macrocycle bond distances range from 2.025(3) to 2.064(2) Å, and the axial Co(2)−O(4) distance is shorter (1.981(2) Å).

In the bulk, the complex has a dimer structure formed by two $[CoCo(L^{2,3})(AcO)]^+$ cations stacked at the open face of the Co(salen) entity. The interdimer Co(1)- -Co(1′) separation is 3.804(1) Å.

General Properties. (a) IR Spectra. Each of **1**−**6** shows the antisymmetric and symmetric ν(COO) modes of the acetate group at ∼1560 and ∼1400 cm^{-1}, respectively. The small separation between the two vibration modes (<200 cm^{-1}) is in harmony with the bridging function of the acetate group.[29] The ν(C═N) vibration is seen at 1640−1630 cm^{-1}. The ν_3 mode of the perchlorate group splits into two, suggesting a weak interaction of the ion in the crystal lattice. The ν_4 mode of the ion is located at ∼620 cm^{-1}.

(b) Magnetic Properties. The room-temperature magnetic moments of **1**−**6** are given in the Experimental Section. The magnetic moments of **5** and **6** (CoZn) clearly indicate that the Co^{II} in the salen site is of low-spin ($S = {}^1/_2$). The magnetic moments of **1** and **2** (CoMn) and **3** and **4** (CoCo) suggest that the Co^{II} in the salen site is of low-spin ($S = {}^1/_2$), and the M^{II} in the saltn or salbn site is of high-spin ($S = {}^5/_2$ for Mn^{II} and ${}^3/_2$ for Co^{II}).[6−9] The moments of **1**−**4** slightly decrease with decreasing temperature. As a first approximation, this may be ascribed to an antiferromagnetic spin-exchange between the Co^{II}−M^{II} pair. However, we have noticed that the CoZn complexes (**5** and **6**) also show a significant temperature dependence in magnetic moment: **5**, 2.30 μ_B at 290 K and 1.37 μ_B 80 K; **6**, 1.90 μ_B at 290 K and 1.22 μ_B at 80 K. An origin for the reduced magnetic moments of **5** and **6** must be an intermolecular antiferromagnetic spin-exchange between low-spin Co^{II} ions in the stacked form (see Figure 2). In addition to this, low-spin Co^{II} of four- or five-coordination generally shows a temperature dependence of the magnetic moment due to an orbital contribution from low-lying excited states.[30] In the case of **3** and **4**, the zero-field splitting of the high-spin Co^{II} in the saltn or salbn site can be an origin for the lowering of magnetic moment. For these reasons, detailed magnetic analyses of the complexes were not made in this work.

(c) ESR Spectra. No ESR signal was observed for **1**−**4**, probably due to magnetic interaction within the dinuclear core. On the other hand, well-resolved ESR spectra were obtained for **5** and **6** when measured in frozen DMF solution: **5**, $g_\perp = 2.21$, $g_\parallel = 2.00$, $A_\perp = 99.0$ G, and $A_\parallel = 116.4$ G; **6**, $g_\perp = 2.23$, $g_\parallel = 1.99$, $A_\perp = 99.0$ G, and $A_\parallel = 117.4$ G. The spectra are typical of low-spin Co^{II} having one unpaired electron on the d_{z^2} character orbital.[31]

(d) Electronic Spectra. Electronic spectra of **1**−**6** were studied in DMF at ambient temperature. All of the complexes are similar in their spectral features in the region 340−700 nm and show an intense band at ∼360 nm and two moderately intense bands at ∼440 and ∼540 nm. The former intense band can be assigned to the $\pi-\pi^*$ transition associated with the azomethine group.[32,33] The moderately intense band can be assigned to charge-transfer bands associated with the Co^{II} in the salen site.

When studied at a higher concentration (∼2 × 10^{-2} M), complexes **1**−**3** show a band maximum at 1250 nm (ϵ ∼15 M^{-1} cm^{-1}) and a discernible shoulder near 1050 nm (ϵ 5−10 M^{-1} cm^{-1}). This spectral feature is characteristic of five-coordinate derivatives of Co(salen), such as $[Co(salen)]_2$ and [Co(salen)Py], and two bands are assigned to the d−d components of the low-spin Co^{II} ion.[31,34,35] Complex **4** also shows two near-IR bands, with a band maximun at 1050 nm (ϵ ∼15 M^{-1} cm^{-1}) and a shoulder at 1250 nm (ϵ ∼10 M^{-1} cm^{-1}). The near-IR spectra of the CoZn complexes **5** and **6** could not be obtained because of the low solubility of the complexes in DMF.

(e) Cyclic Voltammograms. The electrochemical properties of **1**−**6** were studied by cyclic voltammetry. The complexes resemble each other in redox behavior and show an irreversible or quasi-reversible couple at −0.3 V (vs Ag/Ag$^+$) and a reversible couple at ∼−1.3 V. The two waves are ascribed to the Co in the salen site; Zn^{II} is electrochemically inert, and Mn^{II} and Co^{II} in the saltn or salbn site are hardly reduced at the available potential.[9] The wave at ∼ −0.3 V is attributed to the Co^{II}/Co^{III} process.[36] Co^{III} generally prefers an octahedral geometry, and the poor reversibility of the wave is related to the geometrical change at the Co center in the redox process. The couple at ∼ −1.3 V can be attributed to the Co^{II}/Co^{I} process.[36] The good reversibility of the process can be understood because both low-spin Co^{II} (d^7) and Co^{I} (d^8) prefer an axially distorted geometry.

Oxygenation Behavior. Oxygenation of **1**−**6** in DMF was studied by means of electronic spectral and NMR techniques. The introduction of dioxygen into a DMF solution of **1** (CoMn) at 0 °C caused an immediate color change from red to dark red and showed a fairly intense band near 600 nm (ϵ 2310 M^{-1}cm^{-1}) characteristic of the Co(salen)/O_2 adduct[37,38] (Figure 5, trace b). When the solution was purged with argon, the spectrum of **1** was recovered (trace a). The result indicates reversible oxygenation of **1** at this temperature. When the oxygenated solution was warmed to room temperature, the dark red color of the solution gradually faded to yellow in 2 h, probably due to irreversible oxidation. The oxidized yellow solution showed no absorption in the visible region (trace c). Similar reversible oxygenation at 0 °C and irreversible oxidation at room temperature were recognized for **2**, **4**, **5**, and **6**. It must be emphasized that the oxygenated species of these complexes show electronic spectra very similar to trace b, indicating the oxygenated species formed at 0 °C to be same for all these complexes.

To specify the oxygenated species in solution, ESR spectra for the oxygenated solutions were examined. The ESR spectrum

(28) Addison, A. W.; Rao, T. N.; Reedijk, J.; Rijn, J. V.; Verschoor, G. C. *J. Chem. Soc., Dalton Trans.* **1984**, 1349.
(29) Deacon, G. B.; Phillips, R. J. *Coord. Chem. Rev.* **1980**, *33*, 227.
(30) Boudreaux, E. A.; Mulay, L. N. *Theory and Applications of Molecular Paramagnetism*; Wiley: New York 1976; pp 220−223.
(31) Nishida, Y.; Kida, S. *Coord. Chem. Rev.* **1979**, *27*, 275.
(32) Bosnich, B. *J. Am. Chem. Soc.* **1968**, *90*, 627.
(33) Downing, R. S.; Urbach, F. L. *J. Am. Chem. Soc.* **1969**, *91*, 5977.
(34) Yamada, S. *Coord. Chem. Rev.* **1966**, *1*, 415.
(35) Hitchman, M. A. *Inorg. Chem.* **1977**, *16*, 1985.
(36) Costa, G.; Puxeddu, A.; Bardin Stefani, L. *Inorg. Nucl. Chem. Lett.* **1970**, *6*, 191.
(37) McLendon, G.; Martell, A. E. *Coord. Chem. Rev.* **1976**, *19*, 1.
(38) Nakamoto, K.; Oshio, H.; Ōkawa, H.; Kanda, W.; Horiuchi, K.; Kida, S. *Inorg. Chim. Acta* **1985**, *108*, 231.

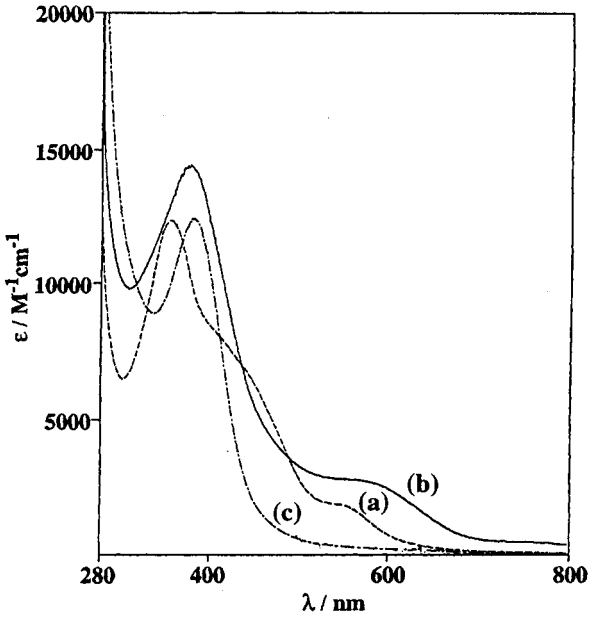

Figure 5. Electronic spectra for **1** in DMF: (a) **1** in the absence of O_2; (b) **1** oxygenated at 0 °C; (c) the oxygenated solution warmed to room temperature (after 2 h).

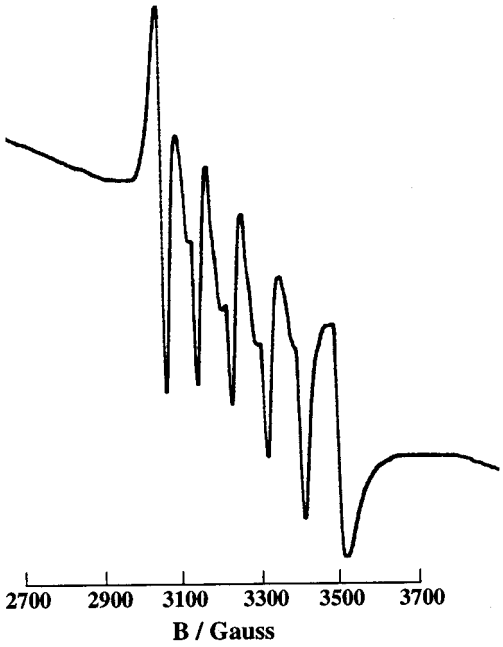

Figure 6. ESR spectrum of the oxygenated complex of **1** (in frozen DMF solution).

for the oxygenated solution of **1** shows a well-resolved six-line signal at $g \sim 2$ (Figure 6) attributable to isolated Mn^{II}. The result clearly indicates the oxygenated species to be a peroxo dimer $[\{Co^{III}Mn^{II}(L^{2,3})(AcO)\}_2(O_2^{2-})]^{2+}$ with an intermolecular $Co^{III}-O-O-Co^{III}$ linkage. A similar ESR spectrum was obtained for the oxygenated solution of **2**. The ESR spectrum of the oxygenated solution of **4** was not well-resolved. The oxygenated solutions of **5** and **6** were ESR-silent in accord with the peroxo dimer formation. In our recent X-ray crystallographic study for oxygenation of a $Co^{II}Co^{II}$ complex derived from a related macrocycle, the formaton of a peroxo dimer at the Co(salen) site has clearly been demonstrated.[39]

(39) Furutachi, H.; Fujinami, S.; Suzuki, M.; Ōkawa, H. *Chem. Lett*. **1998**, 779.

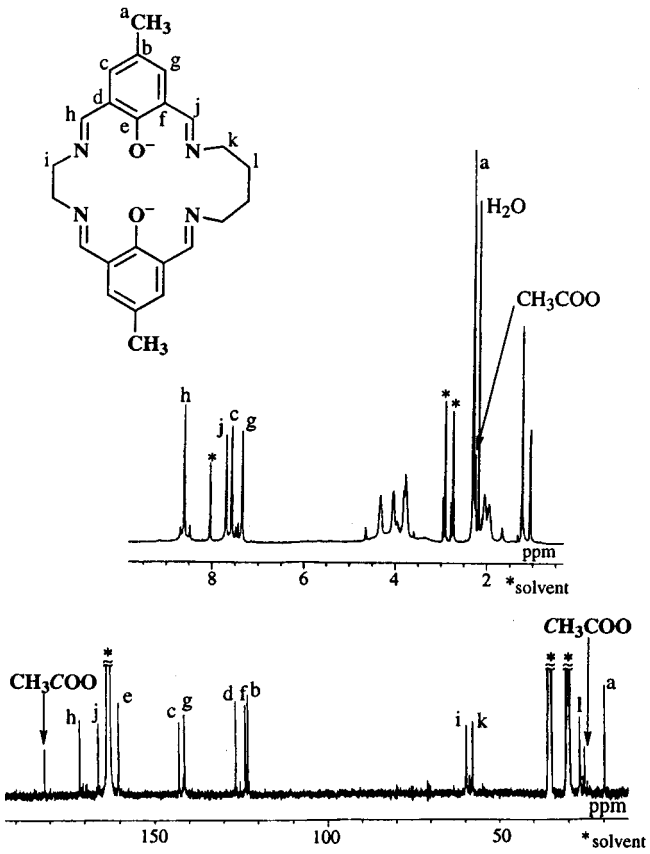

Figure 7. ^1H NMR (top) and ^{13}C NMR (bottom) spectra for the oxygenated solution of **6** in DMF-d_7 at −20 °C.

The formation of the peroxo dimer $[\{Co^{III}M^{II}(L)(AcO)\}_2(O_2^{2-})]^{2+}$ is supported by the NMR studies on the oxygenated solutions of **5** and **6**. ^1H and ^{13}C NMR spectra for the oxygenated solution of **6** (in DMF-d_7 at −20 °C) are given in Figure 7.

Azomethine protons h and j appear at different resonances in accord with the unsymmetric nature of the macrocycle and the core structure (see Figure 4). Ring protons c and g also appear at different resonances. The ^{13}C NMR spectrum of the peroxo complex of **6** exhibits 12 carbon resonances of higher intensity (19.7, 26.8, 57.8, 59.7, 123.0, 123.7, 126.5, 141.4, 142.9, 160.3, 166.0, 171.3 ppm) and two resonances of weaker intensity (25.4 and 181.4 ppm). The two weaker resonances are assigned to the acetate carbons. The 12 resonances of higher intensity are assigned to the nonequivalent carbons of the macrocycle in C_2 symmetry. The ^1H and ^{13}C NMR spectral features clearly demonstrate that the two $\{CoZn(L^{2,4})\}$ moieties of the peroxo complex are equivalent in solution, indicating the free rotation of the two moieties about the Co−O−O−Co linkage in the respective NMR time scales.

The irreversible oxidation of the peroxo complexes of **1**, **2**, **4**, **5**, and **6** at room temperature may proceed through the hydrolytic replacement of the peroxo group to form a $Co^{III}M^{II}$ species.

Complex **3**, on the other hand, is highly sensitive to molecular dioxygen. Soon after being oxygenated at 0 °C, the solution assumed a deep red color and showed band maxima at 375 (ϵ 11 390 M^{-1} cm^{-1}) and 580 nm (ϵ 1290 $M^{-1}cm^{-1}$) (see Figure 8). This spectrum resembles trace b of Figure 5, indicating that the peroxo dimer $[\{Co^{III}Co^{II}(L^{2,3})(AcO)\}_2(O_2^{2-})]^{2+}$ is formed as a dominant species. However, the color of the solution faded within 30 min, and the resulting yellow solution showed a spectrum similar to trace c of Figure 5. The short lifetime of

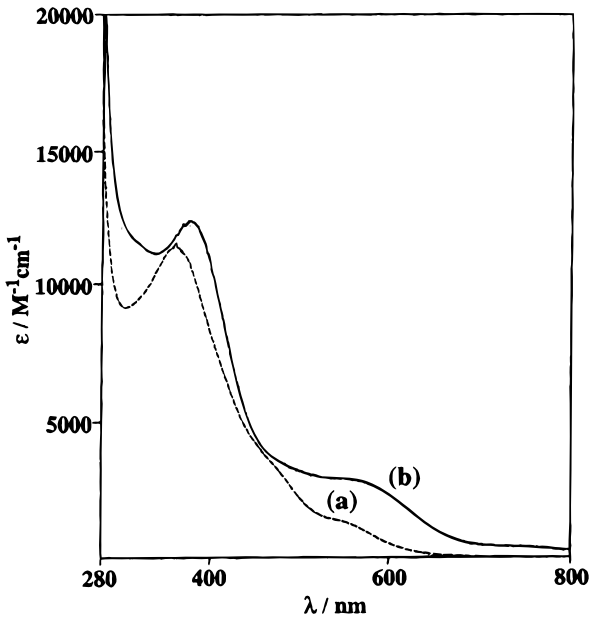

Figure 8. Visible spectra of **3** (a) and its oxygenated complex (b) at 0 °C.

the peroxo complex suggests that **3** is oxidized by a mechanism differing from the peroxo dimer formation discussed above. Eventually, we noticed the lifetime of the peroxo complex of **3** to vary with the solution concentration; the higher the concentration, the longer the lifetime. This reminds us that peroxo and superoxo species exist in equilibrium in solution,[40] i.e.

$$[Co^{II}Co^{II}(L)(AcO)]^+ + O_2 \rightleftharpoons [Co^{III}Co^{II}(L)(AcO)(O_2^-)]^+$$

$$[Co^{III}Co^{II}(L)(AcO)(O_2^-)]^+ + [Co^{II}Co^{II}(L)(AcO)]^+ \rightleftharpoons [\{Co^{III}Co^{II}(L)(AcO)\}_2(O_2^{2-})]^{2+}$$

If the superoxo terminal oxygen of $[Co^{III}Co^{II}(L^{2,3})(AcO)(O_2^-)]^+$ makes a bond with the adjacent Co^{II} ion within a molecule, an intramolecular-type peroxo complex $[Co^{III}Co^{III}(L)(AcO)(O_2^{2-})]^+$ is formed. The peroxo bridge over the CoCo core at the open face seems feasible for **3** on the basis of the X-ray crystallographic results (Figure 4). The superoxo complex may exist as a minor species in an equilibrium, but **3** can be oxidized through the intramolecular-type peroxo complex into a Co^{III}-Co^{III} species if the peroxo complex is unstable at ~0 °C. It must be mentioned why **4** is not oxidized through such an intramolecular-type peroxo complex. It is likely that the Co^{II} in the salbn site is too large to accommodate low-spin Co^{III} (ionic radius for six-coordination; 0.67 Å[41]). In the case of **5** and **6**, the irreversible oxidation through the intramolecular-type peroxo complex is ruled out because the Zn^{II} in the saltn or salbn site cannot be involved in the two-electron reduction of dioxygen because of its redox inertness. In the case of **1** and **2**, the intramolecular-type peroxo complex cannot be formed because the Mn^{II} is largely displaced from the mean molecular plane toward the closed face (see Figure 4).

Scheme 1. Oxygenation and Oxidation Behavior of **1**−**6**.

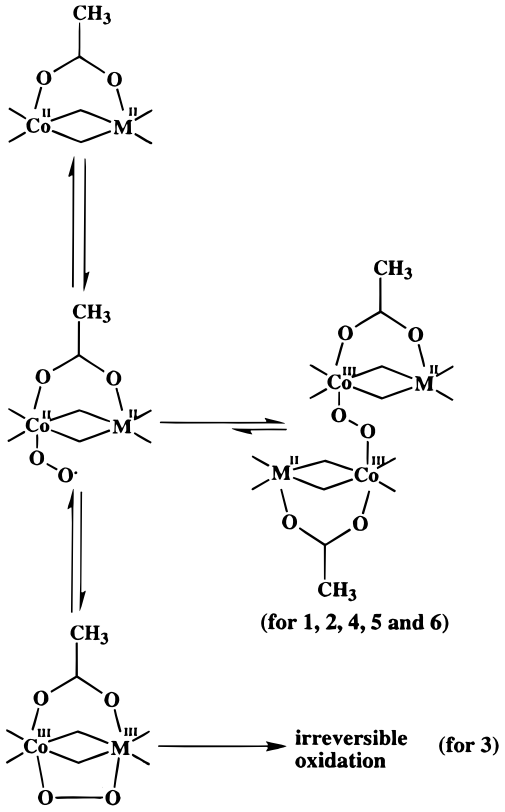

The oxygenation and oxidation behavior of the Co^{II}M^{II} complexes is summarized in Scheme 1. The present study indicates that the reactivity of the Co^{II}M^{II} complexes toward molecular dioxygen at the Co(salen) center is influenced by the neighboring M^{II} ion and the Co^{II}M^{II} core structure.

Acknowledgment. This work was supported by Grants-in-Aid for Scientific Research (No. 09440231), for Scientific Research in the Priority Area of Metal-Assembled Complexes (No. 10149106), and for an International Scientific Research Program (No. 09044093) from the Ministry of Education, Science, and Culture of Japan.

Supporting Information Available: X-ray crystallographic files, in CIF format, for **1**, **2′**, **3**, and **5**. This material is available free of charge via the Internet at http://pubs.acs.org.

IC9809456

(40) Ochiai, E. *J. Inorg. Nucl. Chem.* **1973**, *35*, 1727.
(41) Shannon, R. D.; Prewitt, C. T. *Acta Crystallogr., Sect. B* **1969**, *25*, 925.